FLAME ACCELERATION IN STOICHIOMETRIC METHANE/HYDROGEN/AIR MIXTURES IN AN OBSTRUCTED CHANNEL: EFFECT OF HYDROGEN BLEND RATIO

Chenyuan Cai, Jizhou Dong, Mingbin Zhao, Lei Liu, Min Li and Huahua Xiao
State Key Laboratory of Fire Science, University of Science and Technology of China, 443 Huangshan Road, Hefei, 230027, China, xiaoh@ustc.edu.cn

ABSTRACT

Experiments and numerical simulations were conducted to study the flame acceleration (FA) in stoichiometric CH_4/H_2/air mixtures with various hydrogen blend ratios (i.e., *Hbr* = 0%, 20%, 50%, 80%, and 100%). In the experiments, high-speed photography was used to record the FA process. In the calculations, the two-dimensional, fully-compressible, reactive Navier-Stokes equations were solved using a high-order algorithm on a dynamically adapting mesh. The chemical reaction and diffusive transport of the mixtures were described by a calibrated chemical-diffusive model. The numerical predictions are in good agreement with the experimental measurements. The results show that the mechanism of FA is similar in all cases, that is the flame is accelerated by the thermal expansion effects, various fluid-dynamic instabilities, flame-vortex interactions, and the interactions of flame with pressure waves. The hydrogen blend ratio has a significant impact on the propagation speed and the morphological evolution of the flame during FA. A larger hydrogen blend ratio leads to a faster FA, and the difference in FA mainly depends on the increase of flame surface area and the interactions between flame and pressure waves. In addition, as the hydrogen blend ratio increases, there are fewer pockets of the unburned funnels in the combustion products when the flame propagates to the end of the channel.

Keywords: CH_4/H_2/air mixture; Flame acceleration; Obstructed channel; Simulation; Experiment

1.0 INTRODUCTION

Hydrogen is widely regarded as a promising alternative fuel because of its advantages such as high energy efficiency and ultra-low harmful emissions [1-3]. However, hydrogen has a high risk of fires and explosions due to its extremely lower ignition energy, wide flammability range, higher laminar burning velocity, and great propensity for leakage [4,5]. Hydrogen transportation and storage is one of the most challenging problems. One solution to this problem is to blending hydrogen into natural gas in the existing pipeline network. This is recognized as an efficient way to transport and store hydrogen, and CH_4-H_2 binary fuel is considered to be an important means of hydrogen utilization [6]. As a flammable gas, CH_4-H_2 binary fuel usually forms a laminar flame initially once it is mixed with air and ignited by a small spark. The laminar flame may evolve into a turbulent flame and even undergo a transition to detonation under certain conditions [7-9]. A detonation has a huge destructive potential to life and property because very high overpressure up to several tens of bars can be generated. The initiation of detonation usually arises in a relatively small local region of unburned gas mixture whose thermodynamic state has been conditioned by the flame acceleration (FA) process. Therefore, the study of the FA process is as important as detonation in connection with hydrogen safety.

The propagation of premixed flame in a channel is a highly complicated and dynamic process. Extensive investigations have been conducted to understand this complex FA process in a smooth tube [9-12]. A freely expanding flame is intrinsically unstable. The initially smooth surface of a laminar flame can become wrinkled due to the Landau–Darrieus instability, which can be stabilized or destabilized by the thermal-diffusion effects [9]. The thermal expansion effect of the combustion products produces movement in the unburned gas. This leads to a moderate increase in the flow velocity and flame speed. Then the interactions of flame with the boundary layer and pressure waves under changing background conditions become the dominant factors in the late stage of FA [9,13]. If obstacles are present in a smooth channel, vortices can be produced, which facilitates the increase of flow disturbances, promotes the generation of turbulent flames, and therefore results in a faster FA [9]. Various fluid-dynamic instabilities (e.g., the Kelvin-Helmholtz, Rayleigh-Taylor, and Richtmyer-Meshkov instabilities), flame-vortex and flame-shock interactions can induce additional flame surface area and heat release

rate, and further enhance the FA process [8,9]. In addition, a powerful jetflow created by delayed burning between the obstacles was found to be able to drive FA [14].

Numerous studies have been devoted to the characteristics of flame propagation and acceleration in CH_4-H_2 binary fuel. Ciccarelli et al. [15] performed experiments to find the critical mixture composition required for FA to a fast-flame in CH_4/H_2/air mixtures. The results show that the critical expansion ratio ranges between 2 and 4 for H_2-air mixtures and ups to 8 for CH_4-air mixtures at an initial temperature of 573 K. The detonation of mixed fuels was studied experimentally by Takita et al. [16]. They found that the detonation induction time of the mixture with a lower sensitivity (e.g., CH_4-air mixtures) can be considerably reduced by adding a small amount of another fuel with a higher sensitivity. Hsu et al. [17] conducted experimental research to investigate FA in stoichiometric CH_4/H_2/O_2 mixtures in millimeter-scale smooth tubes. It was discovered that detonation occurs when the molar fraction of CH_4 in a 3.0 mm tube exceeds 0.3. There are three phases in the early stages of flame propagation: constant velocity propagation, deceleration, and exponential acceleration. Recently, the detonation characteristics of CH_4-H_2 binary fuels have been explored. Sun et al. [18] and Li et al. [19] analysed the flame velocity and detonation cell size of CH_4/H_2/O_2 mixtures in the channel with obstacles located at different configurations, while Porowski et al. [20] and Wang et al. [21] carried out the similar study for CH_4/H_2/air mixtures. To examine the detonation limits behaviour, the velocity deficit, cellular structure, and induction length of CH_4/H_2/O_2 mixtures were studied by Zhang et al. [22-24]. In addition, Shamshin et al. [25] evaluated the deflagration-to-detonation transition (DDT) run-up distance and time in stoichiometric CH_4/H_2/air mixtures with hydrogen blend ratio between 0 and 1, and found that the dependence of DDT run-up distance and time on hydrogen blend ratio is nonmonotonic. Based on the studies mentioned above, it can be concluded that the current research about CH_4-H_2 binary fuels is mainly focused on detonation, while studies related to the effect of hydrogen addition on FA remain few.

The purpose of this study is to investigate the effects of hydrogen addition on FA in stoichiometric CH_4/H_2/air mixtures in a channel with triangular obstacles by experiments and simulations. The FA process in the experiments was recorded by high-speed photography. The numerical simulations were performed by solving the two-dimensional (2D), unsteady, fully-compressible, reactive Navier-Stokes (N-S) equations using a fifth-order numerical algorithm and adaptive mesh refinement (AMR).

2.0 METHODOLOGY

2.1 Experimental setup

Figure 1 shows the schematic of the experimental setup, which mainly consists of a constant-volume combustion channel, a high-speed schlieren photography system, a gas mixing device, a high-voltage spark ignition system, a data acquisition system, and a synchronization controller. The combustion channel is a rectangular duct with a length of 30 cm and a cross-section of 2 cm × 2 cm. Continuous triangular obstacles that are 5.8 mm wide and 3 mm high are installed in the channel along the upper and bottom walls. All the experiments were performed using stoichiometric CH_4/H_2/air mixtures with different hydrogen blend ratios of 0%, 20%, 50%, 80%, and 100%, which were controlled by the high-precision mass flow meters in the gas mixing device. The premixed gases initially at 298 K and 101325 Pa were ignited by an electric spark, which is located on the central axis and 5.8 mm away from the left end wall.

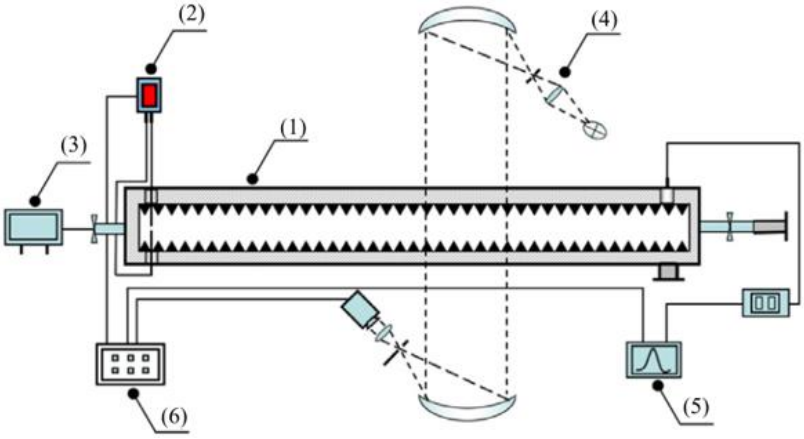

Figure 1. Sketch of experimental setup: (1) combustion channel; (2) spark ignition system; (3) gas mixing device; (4) high-speed schlieren photography system; (5) data acquisition system; (6) synchronization controller

2.2 Numerical methods

The numerical simulations use a fifth WENO scheme with HLLC fluxes [26] and a second-order Runge-Kutta algorithm to solve the 2D reactive N-S equations [27-29]:

$$\frac{\partial \rho}{\partial t} + \nabla \cdot (\rho \boldsymbol{U}) = 0, \tag{1}$$

$$\frac{\partial (\rho \boldsymbol{U})}{\partial t} + \nabla \cdot (\rho \boldsymbol{U}\boldsymbol{U}) + \nabla p = \nabla \cdot \hat{\tau}, \tag{2}$$

$$\frac{\partial (\rho E)}{\partial t} + \nabla \cdot \big((\rho E + p)\boldsymbol{U}\big) = \nabla \cdot (\boldsymbol{U} \cdot \hat{\tau}) + \nabla \cdot (K \nabla T) - \rho q \dot{\omega}, \tag{3}$$

$$\frac{\partial (\rho Y)}{\partial t} + \nabla \cdot (\rho Y \boldsymbol{U}) = \nabla \cdot (\rho D \nabla Y) + \rho \dot{\omega}, \tag{4}$$

$$p = \rho R T / M, \tag{5}$$

$$E = \frac{p}{\rho(\gamma - 1)} + \frac{1}{2}\boldsymbol{U}^2, \tag{6}$$

where ρ - density, kg/m^3; t - time, s; $\boldsymbol{U}$ - velocity, m/s; p - pressure, Pa; E - specific total energy, J/kg; K - thermal conductivity, J/(s·m·K); T- temperature, K; q - chemical energy release, J/kg; $\dot{\omega}$ - chemical reaction rate, mol/s; Y - reactant mass fraction, mol; D - mass diffusivity, m^2/s; R - universal gas constant, J/(mol·K); M - molecular weight, kg/mol; and γ - specific heat ratio. The viscous stress tensor is calculated as $\hat{\tau} = \rho \upsilon((\nabla \boldsymbol{U}) + (\nabla \boldsymbol{U})^{Tr} - \frac{2}{3}(\nabla \cdot \boldsymbol{U})I)$, where ν - kinematic viscosity, Pa·s; I - unit tensor, and Tr denotes matrix transposition.

The conversion from reactants to combustion products as well as the chemical energy release [28] is modeled by using a simplified, calibrated chemical-diffusive model (CDM). The chemical reaction rate is expressed as: $\dot{\omega} \equiv \frac{dY}{dt} = -A\rho Y exp(-\frac{E_a}{RT})$, where E_a - activation energy, J/mol; A - pre-exponential factor, m^3/(kg·s). The dynamic viscosity, mass diffusivity, and thermal diffusivity are presented as [28]: $\upsilon = \upsilon_0 \frac{T^{0.7}}{\rho}$, $D = D_0 \frac{T^{0.7}}{\rho}$, $\frac{K}{\rho c_p} = \kappa_0 \frac{T^{0.7}}{\rho}$, where ν_0, D_0 and κ_0 - reference coefficients, kg/(s·m·K$^{0.7}$); c_p – heat capacity, J/(kg·K). The input parameters of CDM and the main properties of the combustion wave for stoichiometric CH_4/H_2/air mixtures with various hydrogen blend ratios initially at 298 K and 101325 Pa are summarized in Table 1. The hydrogen blend ratio is defined as follows:

$$(1-x_{H_2})CH_4 + x_{H_2}H_2 + \frac{4-3x_{H_2}}{2}(O_2 + 3.76N_2) = (2-x_{H_2})H_2O + (1-x_{H_2})CO_2 + (7.52 - 5.64x_{H_2})N_2, \quad (7)$$

where x_{H_2} (i.e., *Hbr*) is the mole fraction of hydrogen in the fuel, and are set to 0%, 20%, 50%, 80%, and 100% in this study. The CDM has been extensively tested and applied in the studies including dynamics of laminar and turbulent flames [13,30,31], cellular detonations [32,33], flame-shock interactions and DDT [27,34-36].

Table 1. Input model parameters and output combustion wave properties for stoichiometric CH_4/H_2/air mixtures with various hydrogen blend ratios.

Hbr	0%	20%	50%	80%	100%
Input					
Initial pressure, p_0 (Pa)	101325				
Initial temperature, T_0 (K)	298				
Specific heat ratio, γ	1.1906	1.1905	1.1882	1.1831	1.1790
Molecular weight, M (kg/mol)	0.0274	0.0273	0.0267	0.0256	0.0243
Pre-exponential factor, A ($m^3/(kg\cdot s)$)	3.22×10^{11}	2.60×10^{11}	6.47×10^{10}	2.54×10^{10}	7.52×10^{9}
Activation energy, E_a/RT_0	88.52	85.89	74.17	63.60	53.11
Chemical energy release, qM/RT_0	40.49	40.71	41.62	43.64	46.09
Reference coefficient, $\nu_0 = D_0 = \kappa_0$ ($kg/(s\cdot m\cdot K^{0.7})$)	6.48×10^{-7}	6.84×10^{-7}	7.69×10^{-7}	1.17×10^{-6}	2.53×10^{-6}
Output					
Laminar burning velocity, S_L (m/s)	0.34	0.39	0.55	1.09	2.31
Laminar flame thickness, x_{fT} (mm)	0.46	0.43	0.36	0.30	0.35
Adiabatic flame temperature, T_b (K)	2230	2239	2263	2310	2387
Constant-volume combustion temperature, T_{cv} (K)	2599	2609	2632	2682	2764

The 2D computational domain for the simulations is shown in Figure 2. The channel is filled with stoichiometric CH_4/H_2/air mixtures with different hydrogen blend ratios, which are assumed to be perfectly mixed and behave as an ideal gas. The flame is initialized as a circular region of hot and burned gas with a radius of 1 mm on the centreline of the channel and 5.8 mm from the left end wall. After ignition, the flame expands and propagates from the left to right end of the channel. Adiabatic, no-slip reflecting boundary condition is adopted at the walls and obstacle surfaces: $U = 0$ and $\partial T/\partial n = \partial Y/\partial n = \partial p/\partial n = 0$, where n is the direction normal to the wall. The non-reflecting boundary is applied at the open end of the channel.

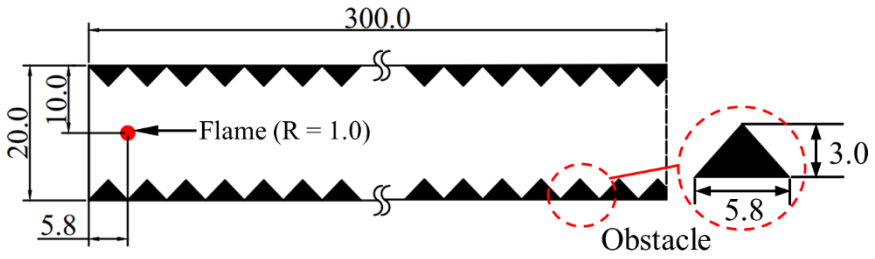

Figure 2. Schematic of computational setup for 2D simulation. Unit is in millimeter.

The AMR technique [37] is used to dynamically refine regions of significant flow features, e.g., flames, boundary layers, and pressure waves. Grid resolution tests were conducted for the stoichiometric CH_4/H_2/air mixture with 80% *Hbr* by changing the minimum cell size (dx_{min}) at the most refined level of the mesh. Figure 3 shows the reaction front speed as a function of flame front position in the case of different minimum grid sizes (1/160, 1/320, and 1/640 cm). It was found that dx_{min} = 1/640 cm is sufficient for simulating the flame propagation for all mixtures with different hydrogen blend ratios.

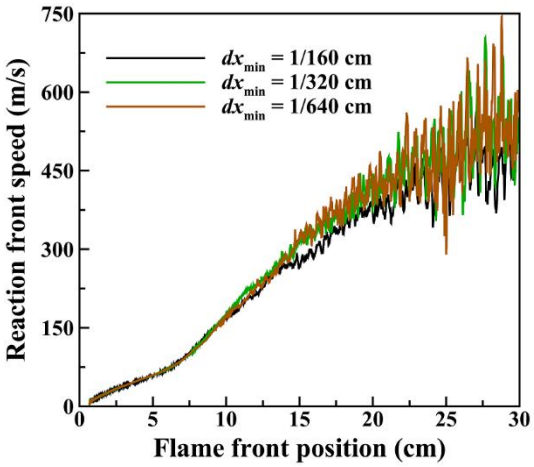

Figure 3. Reaction front speed as a function of flame front position in a stoichiometric CH_4/H_2/air mixture with 80% *Hbr* using different minimum grid sizes.

3.0 RESULTS AND DISCUSSIONS

3.1 Reaction front speed

Figure 4 shows the numerical and experimental reaction front speed as a function of time in stoichiometric CH_4/H_2/air mixtures with different hydrogen blend ratios. The simulated flame propagation speed is in good agreement with the experimental measurements for all cases, particularly in the initial stage of FA. The reaction front speeds undergo a slow increase followed by a very fast increase. The increase of hydrogen addition leads to a more obvious FA progress and causes a relatively faster propagation speed of flame. When the hydrogen blend ratio increases from 0% to 100%, the maximum speed of the reaction front in the simulation increases from about 245.58 m/s to 997.77 m/s, and correspondingly, the duration of the flame propagation process in the 30 cm length channel decreases from about 9.6 ms to 1.5 ms.

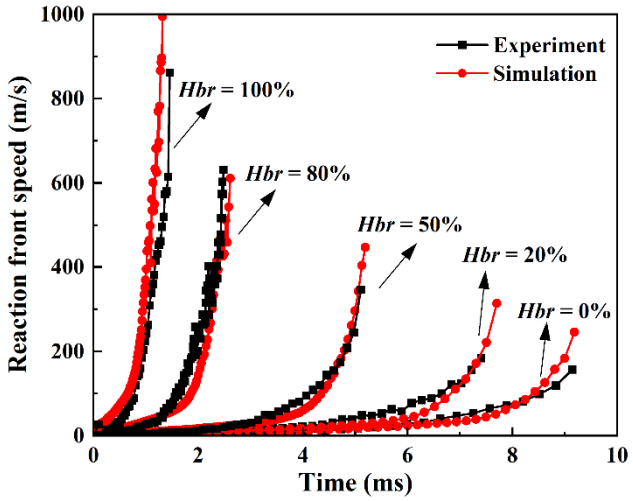

Figure 4. Numerical and experimental reaction front speed as a function of time in stoichiometric CH_4/H_2/air mixtures with various hydrogen blend ratios.

3.2 Overall evolution of flame front

Figure 5 shows the experimental and numerical schlieren images during the flame propagation process at three different stages in stoichiometric CH_4/H_2/air mixtures with various hydrogen blend ratios. The images in the column from left to right correspond to stages 1, 2, and 3, respectively. For comparison, the foremost flame tip reaches approximately the same position along the length of the channel in each stage in the simulations and experiments. Overall, the flame evolution and flow features in the simulations agree well with the experimental observations for all cases. During the initial stage, the flame expands freely after ignition and then spreads rightward and develops into an oval shape, due to the confinement of the wall at the left end and the obstacle surfaces on the upper and lower sides of the channel (see stage 1). In stage 2, the flame wrinkles and distorts as it gets close to the obstacles. The stretching of the flame towards the obstacle gaps becomes more significant in the case with a higher ratio of hydrogen addition. When the flame propagates to the end of the channel, the flame morphologies are different for the mixtures at different hydrogen blend ratios, as shown in stage 3. There are fewer pockets of the unburned gas mixture leaving behind the rapidly accelerating flame front as hydrogen blend ratio increases. Moreover, pressure waves are visible in the fuel mixture with a high ratio of hydrogen in the channel, i.e., *Hbr* = 80% and 100%.

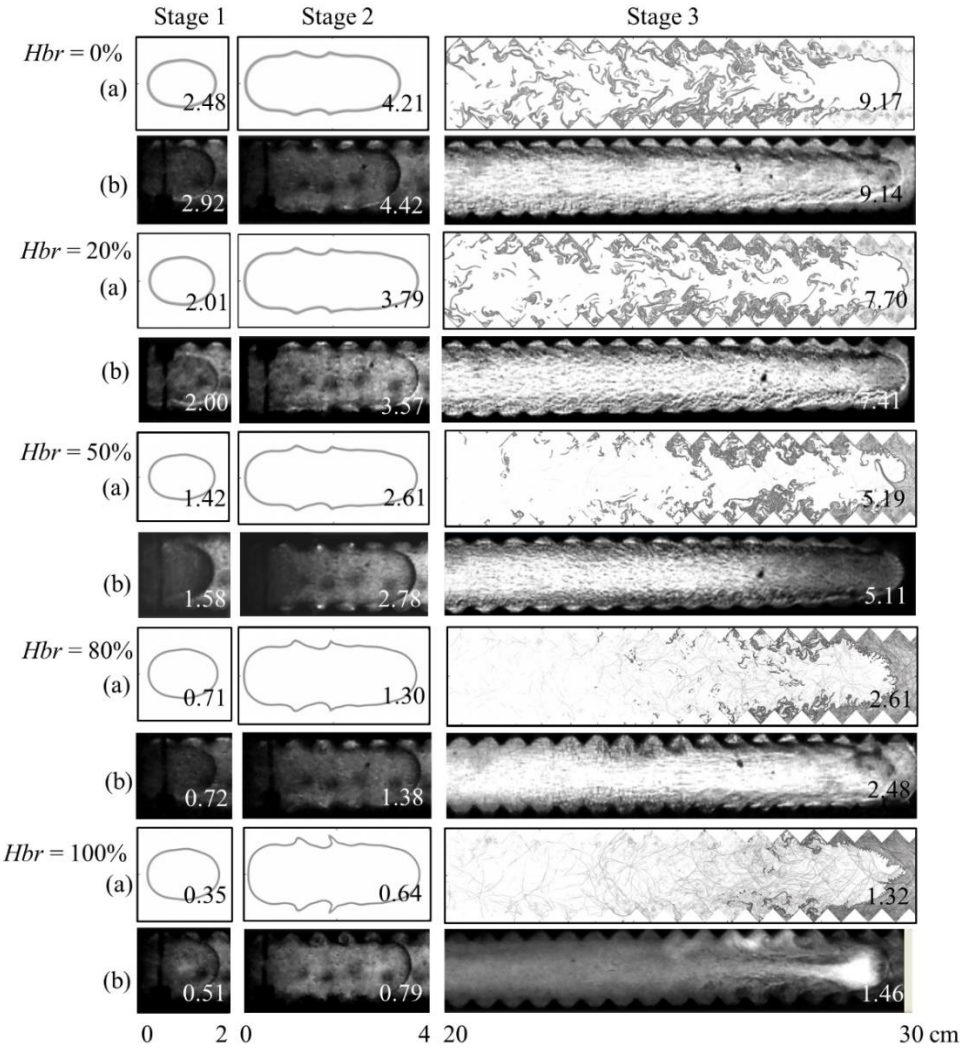

Figure 5. Schlieren images showing flame propagation in stoichiometric CH_4/H_2/air mixtures with various hydrogen blend ratios between (a) simulation and (b) experiments. Time in milliseconds is shown in each frame corner.

3.3 Effect of hydrogen blend ratio

Considering hydrogen blend ratio plays an important role in the flame evolution and acceleration, we explore the effect mechanism of hydrogen blend ratio using numerical simulation. Figure 6 shows the flame propagation process in stoichiometric CH_4/H_2/air mixtures with various hydrogen blend ratios. Each frame consists of a temperature field at the bottom and a schlieren field at the top to show the flame evolution as well as the flow and pressure waves. The flame in each column appears at about the same position in the channel for all cases, that is the flame front in Columns (A), (B) and (C) reaches approximately 8 cm, 14 cm, and 24 cm respectively. As shown in column A, the flames wrinkle and roll up when approaching the obstacles. The entrainment of the flame in the obstacle gaps is more notable as the hydrogen blend ratio increases. The flame entrainment can promote the increase of flame surface area and thus accelerate the flame propagation [38]. In the mixture with 100% *Hbr*, small vortices are formed ahead of the flame front and in the gaps between adjacent obstacles since the unburned gas accelerates quickly over the obstacles. The flame-vortex interaction also leads to a rapid increase in the flame surface area as a result of the flame convolution and fragmentation [39].

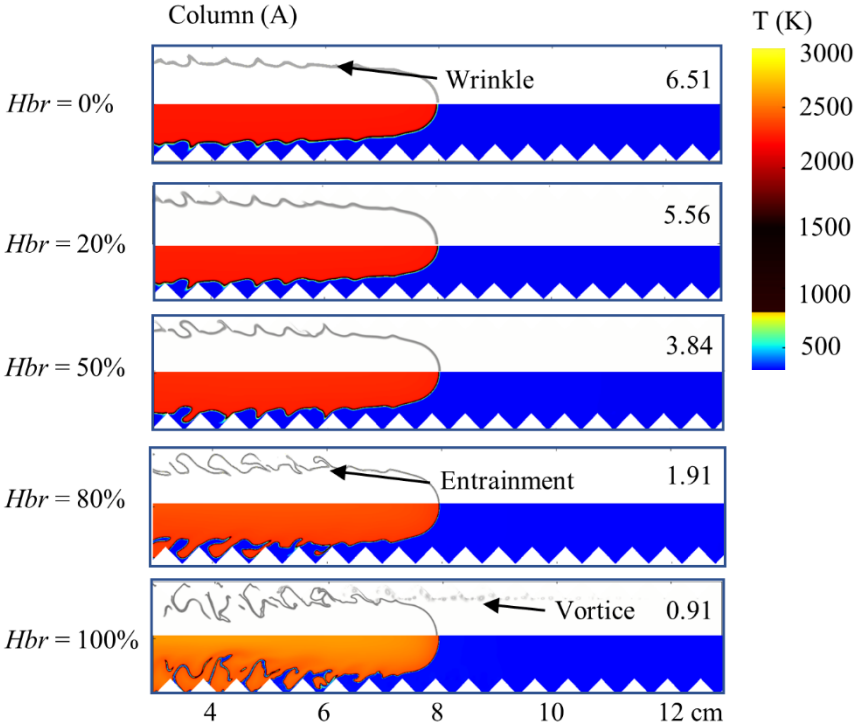

Figure 6. Selected schlieren and temperature fields showing flame propagation process in stoichiometric CH_4/H_2/air mixtures with various hydrogen blend ratios in the obstructed channel. Each frame is a 2 × 10 cm section of the domain, which consists of a schlieren field at the top and a temperature field at the bottom. Time in milliseconds is shown in each frame corner.

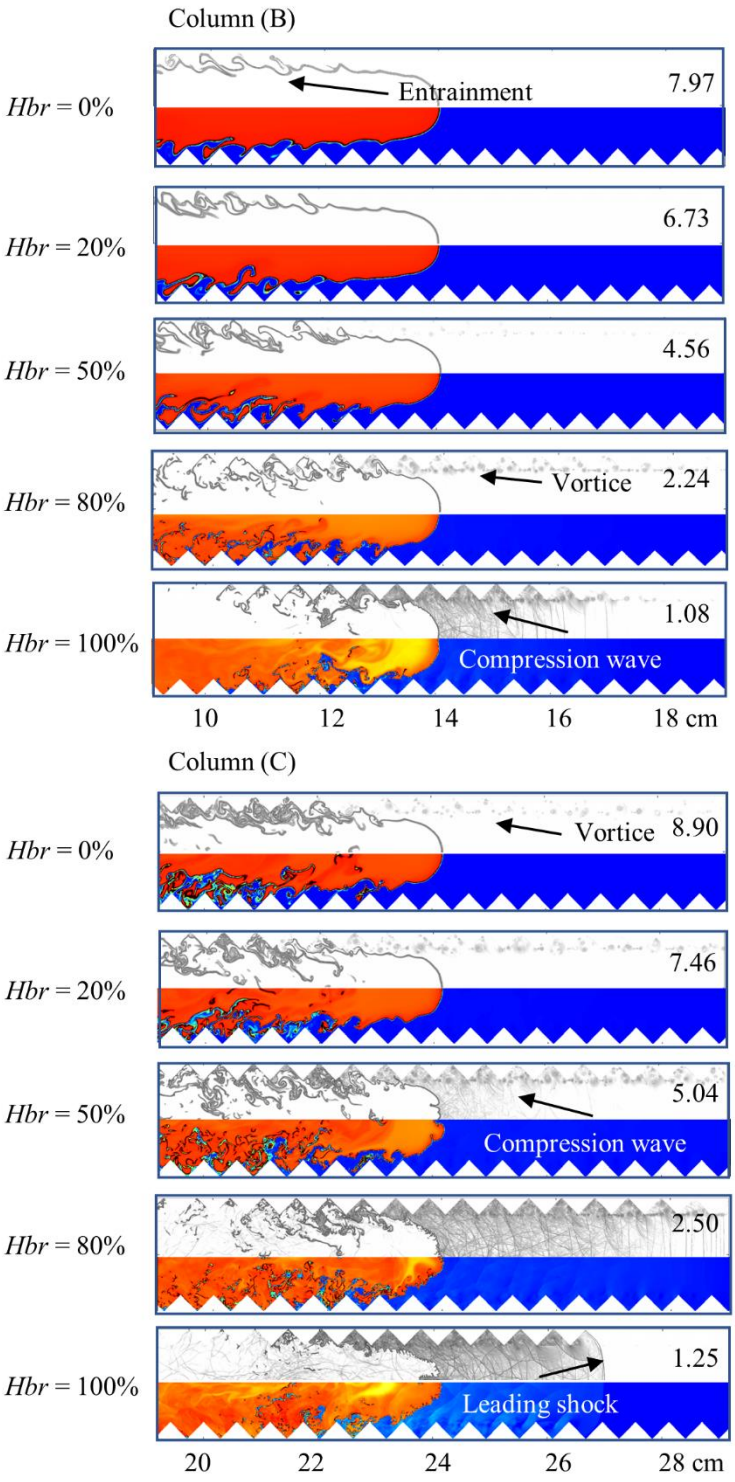

Figure 6. (Continued.)

As the flame accelerates, the flames shown in column B in Figure 6 for the cases with 0%, 20%, and 50% *Hbr* convolute further compared to those in column A. By contrast, small vortices generated can be seen in the obstacle gaps in front of the flame tip in the mixture containing 80% *Hbr*, and weak compression waves are visible in the mixture with 100% *Hbr*. When the flame propagates to the position about 24 cm, as shown in column C in Figure 6, the vortices are larger in the mixtures with a higher hydrogen blend ratio for *Hbr* ≤ 50% because the velocity of the combustion-generated flow increases with a higher ratio of hydrogen blending. For the cases with 50%, 80%, and 100% *Hbr*, the depression

of flame front in the middle and the flame fragmentation are caused by the Richtmyer-Meshkov instability when the compression waves reflect from the obstacles and interact with the flame front. In turn, the flame ripple accelerates the flow, resulting in stronger compression waves. In the case with 100% *Hbr*, a well-defined leading shock resulting from compression wave coalesce appears in the channel.

Figure 7 shows the quantitative relations among reaction front speed, flame surface area, and total heat release rate in stoichiometric CH_4/H_2/air mixtures with different hydrogen blend ratios. Figure 7a displays the reaction front speed as a function of the flame front position. The dashed lines indicate the positions where the flame tips arrive when the flames accelerate to the sound speed of reactants. In general, the flame speed increases with the hydrogen blend ratio. The flame speed fails to reach the sonic velocity of unburned mixture in the cases with *Hbr* $\leqslant$ 20% even if the flame accelerates to the end of the channel. As a result, the compression wave is invisible in the schlieren fields for the cases with *Hbr* $\leqslant$ 20% (see Figure 6). For the case with *Hbr* $\geq$ 50%, the flame propagation speed begins to fluctuate significantly when it reaches the acoustic velocity of unburned gas because the compression waves (as schlieren fields shown in Figure 5) interacting with the flame get stronger as coalescing. Figures 7b and 7c respectively show the variation of flame surface area and total heat release rate with flame front position for various hydrogen blend ratios. The meaning of the dashed lines in Figure 7b is the same as in Figure 7a. As Figure 7b shows, similar to the flame speed shown in Figure 7a, the flame surface area fluctuates around an average value when the flame speed reaches the sound speed of reactants in the cases with *Hbr* $\geqslant$ 50%. The final area of the flame surface decreases with an increasing hydrogen blend ratio. However, this is just the opposite of the trends of total heat release rate with the proportion of hydrogen (as shown in Figure 7c). The reason is that the high reaction rate under the effect of pressure waves helps sustain the heat release rate.

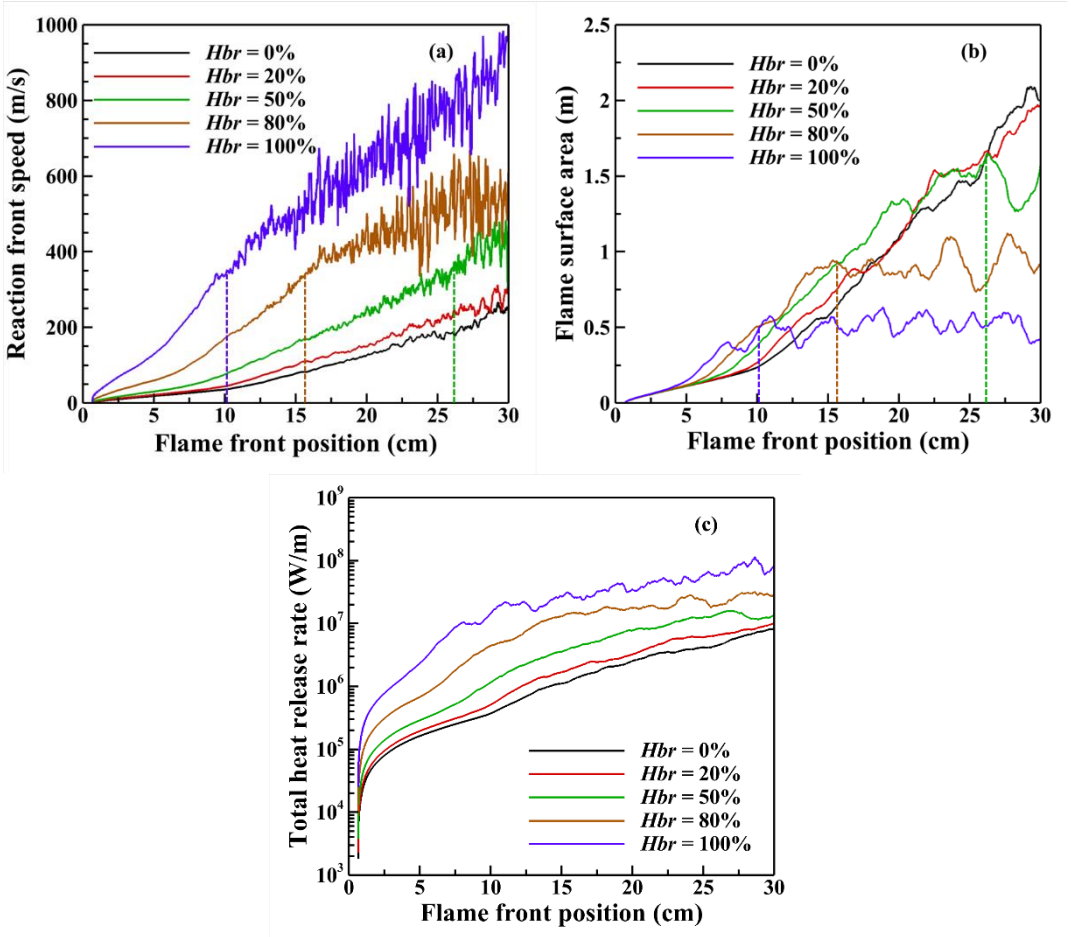

Figure 7. Reaction front speed (a), flame surface area (b), and total heat release rate (c) as a function of flame front position in stoichiometric CH_4/H_2/air mixtures with different hydrogen blend ratios.

4.0 CONCLUSIONS

Experiments and numerical simulations of flame propagation and acceleration process in stoichiometric CH_4/H_2/air mixtures with hydrogen blend ratios of 0%, 20%, 50%, 80%, and 100% in an obstructed channel were conducted. In the experiments, high-speed photography was used to record the propagation of combustion waves. In the numerical calculations, a high-order numerical algorithm was applied to solve the 2D unsteady fully-compressible reactive N-S equations coupled to a calibrated one-step CDM on a locally adapting mesh. The simulations of combustion wave propagation were compared with the experiments. Overall, the calculated results are in reasonable agreement with the experimental measurements.

The study shows that hydrogen addition has a significant impact on the FA process, including the morphological evolution and the propagation speed of the flame. The wrinkle and stretching of the flame towards the obstacle gaps become more significant in the case with a higher ratio of hydrogen addition as the flame gets close to the obstacles. There are fewer pockets of the unburned gas mixture leaving behind the rapidly accelerating flame front as hydrogen blend ratio increases when the flame propagates to the end of the channel. Moreover, pressure waves are visible in the cases with *Hbr* = 80% and 100%. Regarding flame speed, the increase of hydrogen addition leads to a relatively faster propagation and acceleration of the flame. The effect mechanism of the hydrogen blend ratio on FA can be divided into two regimes. First, the flame is governed by the increase of flame surface area as the flame accelerates. Second, the interactions between flame and pressure waves play a dominant role for the further acceleration of the flame when the flame speed reaches the speed of sound in reactants.

The results in this study can be helpful for enriching the FA properties of CH_4-H_2 binary fuels and providing a reference for the effect of hydrogen addition on the FA process as well as the mechanism of FA. Further work remains to be done to explore the influence of hydrogen addition on DDT.

ACKNOWLEDGEMENTS

This study was supported by the Fundamental Research Funds for the Central Universities (Nos. WK2320000055 and WK2320000051) and the National Key R&D Program of China (Grant No. 2021YFB4000902). The authors acknowledge the computing resources provided by the Supercomputing Center of University of Science and Technology of China.

REFERENCES

1. Dincer I, Acar C. Review and evaluation of hydrogen production methods for better sustainability. *International journal of hydrogen energy*, **40**, No. 34, 2015, pp. 11094-11111.
2. Midilli A, Ay M, Dincer I, et al. On hydrogen and hydrogen energy strategies: I: current status and needs. *Renewable and sustainable energy reviews*, **9**, No. 3, 2005, pp. 255-271.
3. Verhelst S, Wallner T. Hydrogen-fueled internal combustion engines. *Progress in energy and combustion science*, **35**, No. 6, 2009, pp. 490-527.
4. Ng H D, Lee J H S. Comments on explosion problems for hydrogen safety. *Journal of Loss Prevention in the Process Industries*, **21**, No. 2, 2008, pp. 136-146.
5. Zheng K, Yu M, Zheng L, et al. Experimental study on premixed flame propagation of hydrogen/methane/air deflagration in closed ducts. *International Journal of hydrogen energy*, **42**, No. 8, 2017, pp. 5426-5438.
6. Ogden J, Jaffe A M, Scheitrum D, et al. Natural gas as a bridge to hydrogen transportation fuel: Insights from the literature. *Energy Policy*, **115**, No., 2018, pp. 317-329.
7. Oran E S, Gamezo V N. Origins of the deflagration-to-detonation transition in gas-phase combustion. *Combustion and Flame*, **148**, No. 1, 2007, pp. 4-47.

8. Ciccarelli G, Dorofeev S. Flame acceleration and transition to detonation in ducts. *Progress in Energy and Combustion Science*, **34**, No. 4, 2008, pp. 499-550.
9. Dorofeev S B. Flame acceleration and explosion safety applications. *Proceedings of the Combustion Institute*, **33**, No. 2, 2011, pp. 2161-2175.
10. Bychkov V, Akkerman V Y, Fru G, et al. Flame acceleration in the early stages of burning in tubes. *Combustion and Flame*, **150**, No. 4, 2007, pp. 263-276.
11. Valiev D M, Akkerman V, Kuznetsov M, et al. Influence of gas compression on flame acceleration in the early stage of burning in tubes. *Combustion and Flame*, **160**, No. 1, 2013, pp. 97-111.
12. Bychkov V, Valiev D, Akkerman V, et al. Gas compression moderates flame acceleration in deflagration-to-detonation transition. *Combustion Science and Technology*, **184**, No. 7-8, 2012, pp. 1066-1079.
13. Xiao H, Houim R W, Oran E S. Formation and evolution of distorted tulip flames. *Combustion and Flame*, **162**, No. 11, 2015, pp. 4084-4101.
14. Bychkov V, Valiev D, Eriksson L E. Physical mechanism of ultrafast flame acceleration. *Physical review letters*, **101**, No. 16, 2008, pp. 164501.
15. Ciccarelli G, Chaumeix N, Mendiburu A Z, et al. Fast-flame limit for hydrogen/methane-air mixtures. *Proceedings of the Combustion Institute*, **37**, No. 3, 2019, pp. 3661-3668.
16. Takita K, Niioka T. On detonation behavior of mixed fuels. *Shock waves*, **6**, No. 2, 1996, pp. 61-66.
17. Hsu Y C, Chao Y C, Chung K M. Flame Propagation in CH4/H2/O2 Blended Mixtures in Smooth Tubes of Millimeter-Scale. *Combustion Science and Technology*, **188**, No. 8, 2016, pp. 1239-1248.
18. Sun X, Li Q, Li C, et al. Detonation propagation characteristics for CH4-2H2-3O2 mixtures in a tube filled with orifice plates. *International Journal of Hydrogen Energy*, **44**, No. 14, 2019, pp. 7616-7627.
19. Li Q, Wei Z, Lv Z, et al. The behaviors of supersonic combustion wave through a perforated plate in a stoichiometric mixtures of H2/CH4/O2 and H2/O2. *Fuel*, **317**, No., 2022, pp. 123092.
20. Porowski R, Teodorczyk A. Experimental study on DDT for hydrogen-methane-air mixtures in tube with obstacles. *Journal of Loss Prevention in the Process Industries*, **26**, No. 2, 2013, pp. 374-379.
21. Wang L Q, Ma H H, Shen Z W, et al. Experimental study of DDT in hydrogen-methane-air mixtures in a tube filled with square orifice plates. *Process Safety and Environmental Protection*, **116**, No., 2018, pp. 228-234.
22. Zhang B, Pang L, Gao Y. Detonation limits in binary fuel blends of methane/hydrogen mixtures. *Fuel*, **168**, No., 2016a, pp. 27-33.
23. Zhang B. Detonation limits in methane-hydrogen-oxygen mixtures: Dominant effect of induction length. *International Journal of Hydrogen Energy*, **44**, No. 41, 2019, pp. 23532-23537.
24. Zhang B, Wang C, Shen X, et al. Velocity fluctuation analysis near detonation propagation limits for stoichiometric methane–hydrogen–oxygen mixture. *International Journal of Hydrogen Energy*, **41**, No. 39, 2016b, pp. 17750-17759.
25. Shamshin I O, Kazachenko M V, Frolov S M, et al. Deflagration-to-detonation transition in stochiometric mixtures of the binary methane-hydrogen fuel with air. *International Journal of Hydrogen Energy*, **46**, No. 68, 2021, pp. 34046-34058.
26. Thornber B, Mosedale A, Drikakis D, et al. An improved reconstruction method for compressible flows with low Mach number features. *Journal of Computational Physics*, **227**, No. 10, 2008, pp. 4873-4894.
27. Kessler D A, Gamezo V N, Oran E S. Simulations of flame acceleration and deflagration-to-detonation transitions in methane-air systems. *Combustion and Flame*, **157**, No. 11, 2010, pp. 2063-2077.
28. Kaplan C R, Ozgen A, Oran E S. Chemical-diffusive models for flame acceleration and transition-to-detonation: genetic algorithm and optimisation procedure. *Combustion Theory and Modelling*, **23**, No. 1, 2019, pp. 67-86.
29. Xiao H, Oran E S. Flame acceleration and deflagration-to-detonation transition in hydrogen-air mixture in a channel with an array of obstacles of different shapes, **220**, No., 2020, pp. 378-393.

30. Poludnenko A Y, Oran E S. The interaction of high-speed turbulence with flames: Global properties and internal flame structure. *Combustion and Flame*, **157**, No. 5, 2010, pp. 995-1011.
31. Poludnenko A Y, Oran E S. The interaction of high-speed turbulence with flames: Turbulent flame speed. *Combustion and flame*, **158**, No. 2, 2011, pp. 301-326.
32. Gamezo V N, Vasil'ev A A, Khokhlov A M, et al. Fine cellular structures produced by marginal detonations. *Proceedings of the Combustion Institute*, **28**, No. 1, 2000, pp. 611-617.
33. Kessler D A, Gamezo V N, Oran E S. Multilevel detonation cell structures in methane-air mixtures. *Proceedings of the Combustion Institute*, **33**, No. 2, 2011, pp. 2211-2218.
34. Xiao H, Oran E S. Shock focusing and detonation initiation at a flame front. *Combustion and Flame*, **203**, No., 2019, pp. 397-406.
35. Gamezo V N, Ogawa T, Oran E S. Flame acceleration and DDT in channels with obstacles: Effect of obstacle spacing. *Combustion and Flame*, **155**, No. 1-2, 2008, pp. 302-315.
36. Goodwin G B, Houim R W, Oran E S. Shock transition to detonation in channels with obstacles. *Proceedings of the Combustion Institute*, **36**, No. 2, 2017, pp. 2717-2724.
37. Boxlib. Center for computational sciences and engineering, University of California, Berkeley, 2015, http://boxlib-codes.github.io/.
38. Ogawa T, Oran E S, Gamezo V N. Numerical study on flame acceleration and DDT in an inclined array of cylinders using an AMR technique. *Computers and Fluids*, **85**, No., 2013, pp. 63-70.
39. Li X, Dong J, Jin K, et al. Flame Acceleration and DDT in a Channel with Continuous Triangular Obstacles: Effect of Blockage Ratio. *Combustion Science and Technology*, 2022.